BNL-228198-2025-JAAM

In Situ Atomic Tracking on the Interfacial Etching and Reconfiguration of Cu-ReSe2 Contact during Thermal Annealing

X. Li, Y. Zhu

To be published in "Nano Letters"

April 2025

Condensed Matter Physics and Materials Science Department

Brookhaven National Laboratory

U.S. Department of Energy

USDOE Office of Science (SC), Basic Energy Sciences (BES)

DISCLAIMER

In-situ Atomic Tracking on the Interfacial Etching and Reconfiguration of Cu-$ReSe_2$ Contact during Thermal Annealing

Xing Li,[1,2,†] Weiwei Yan, [1,†] Dongyang Wang,[1,†] Longbin Yan,[1] Wentao Huang,[1] Xiaoyu Guo,[4] Yao Guo,[4] Shaobo Cheng,[1,3,*] Yimei Zhu,[2,*] Chongxin Shan[1,*]

[1]*Henan Key Laboratory of Diamond Materials and Devices, School of Physics, Zhengzhou University, Zhengzhou 450052, China*

[2]*Condensed Matter Physics and Materials Science Department, Brookhaven National Laboratory, Upton, New York 11973, USA*

[3]*Institute of Quantum Materials and Physics, Henan Academy of Sciences, Zhengzhou, 450046, China*

[4] *School of Physics, Beijing Institute of Technology, Beijing, 100081, China*

† These authors contributed equally to this work.

*Corresponding authors

Email: chengshaobo@zzu.edu.cn; zhu@bnl.gov; cxshan@zzu.edu.cn

Abstract: The Schottky barrier height can be greatly affected by the metal diffusion, reaction and covalent bonding formation at the contact. Exploring novel methods and revealing the fundamental mechanisms for contact engineering is of vital importance for microelectronic devices. Here, the annealing induced interfacial reactions at Cu-$ReSe_2$ contact are dynamically revealed from the atomic scale. Accompanied by the diffusion of Se to Cu, $ReSe_2$ are gradually decomposed to a thin Re interlayer through a "chain-by-chain" manner. Theoretical calculations show that the Cu atoms can facilitate the chemical bond breaking of $ReSe_2$, significantly lowering the Se diffusion energy barrier toward Cu. The formed Re/$ReSe_2$ heterostructure present a metal-like band structure, which underscores the critical role of Cu in altering the interfacial chemistry and promoting carrier transport across the interface. Our results can provide vital insights into the contact properties of $ReSe_2$ and provide a possible method for fabricating high-performance $ReSe_2$-based devices.

Keywords: $ReSe_2$, contact engineering, *in-situ* TEM, interfacial reaction, low-temperature annealing

Introduction

As a 2D material with significant in-plane anisotropy, $ReSe_2$ has recently garnered considerable research interest due to its unique electrical, optical, and phonon properties.[1-4] Unlike other hexagonal transitional metal dichalcogenides (TMDs), the structural distortion (distorted 1*T* phase) of $ReSe_2$ results in much weaker interlayer coupling and a lack of interlayer registry, causing its bulk material to behave electronically and vibrationally as monolayers.[5, 6] However, the formation of Schottky barriers at the metal-TMD interface leads to a persistent challenge for electronic device integration due to the resulting high contact resistance (R_c).[7] It has been reported that the Schottky barrier height can significantly affect the photodetection behavior of $ReSe_2$ and can be modulated by varying hydrogen gas concentrations.[8, 9] Additionally, the thermal stability of the contact also becomes a common reliability issue for device applications. Therefore, understanding the contact degradation mechanism during subsequent processing and packaging steps at elevated temperatures is crucial.[10-13]

Generally, contact resistance can be improved through phase engineering,[7, 14] work function engineering,[15] doping, and clean junctions reconstruction.[16] Thermal annealing has been widely employed to improve the contact by facilitating the removal of defects, passivation of dangling bonds and enhancement of metal-semiconductor bonding.[17-20] The strong covalent bonding between 2D materials and the contact mental can reduce the Schottky barrier height.[21, 22] It has been reported that the contact resistance of $ReSe_2$ field effect transistors can be improved by up to three orders of magnitude with ultra-high-vacuum annealing.[23] However, during the annealing process, metals may react, diffuse, donate charge, or otherwise interact with the TMD film.[7, 24-27] Recently, $ReSe_2$-based memristors with Cu electrodes have been demonstrated, utilizing the mechanism of Cu filament formation and dissolution.[28] Furthermore, Cu atoms can diffuse and intercalate into the lattice of certain 2D materials, forming new hybrid structures.[29, 30] Therefore, understanding the interaction between Cu and TMDs is essential for exploring their combined properties.

In this study, we investigate the interfacial reactions between Cu and layered $ReSe_2$ during the vacuum annealing process via *in-situ* heating experiments. The Cu induced "chain-by-chain" etching of the Re_4 "diamond chains" and the Se diffusion behavior were observed using the aberration-corrected transmission electron microscopy (TEM). The presence of Cu can promote the breaking of Re-Se bond in $ReSe_2$, significantly lowering the energy barrier for Se atom diffusion. The Re/$ReSe_2$

heterostructure exhibits a metal-like electronic band structure, which can facilitate the carrier transport over the interface and can be further utilized to engineer the contact resistance of $ReSe_2$-based devices. Our work provides a comprehensive analysis of the interfacial interactions and structural evolutions between the Cu electrode and $ReSe_2$.

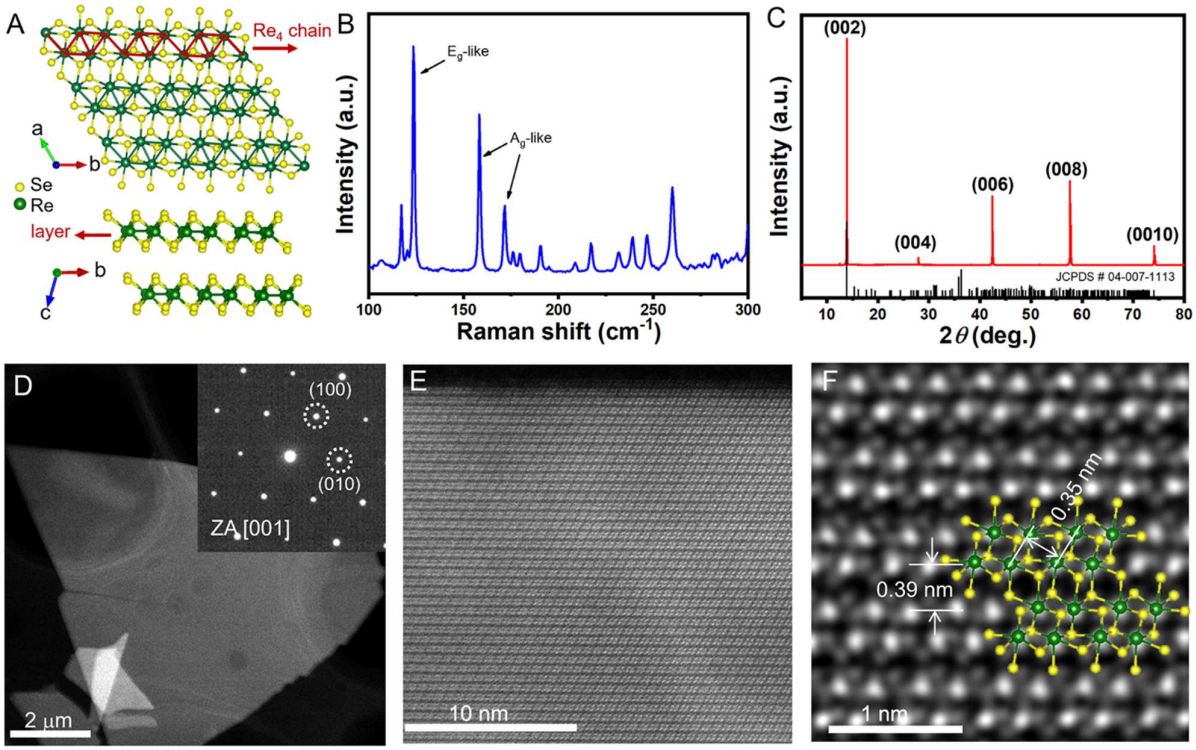

Figure. 1. Crystal structure and characterizations of $ReSe_2$. (A) Schematic illustrations of the crystal structure of $ReSe_2$ in the basal plane and the cross-section view. Four Re atoms form a diamond cluster (green bonds). (B) Raman and (C) XRD spectra of the $ReSe_2$ sample. The patterns were indexed with International Centre for Diffraction Data Powder Diffraction Files 04-007-1113. (D) The morphology and corresponding SAED pattern of the exfoliated $ReSe_2$ flake. (E) The low- and (F) high-mag HAADF-STEM images of the $ReSe_2$ flake.

Results and Discussion

Figure 1A presents the distorted 1T structure of $ReSe_2$ with the Re_4 units form a 1D chain along the ***b*** [010] direction within each monolayer. The angle between ***a***-axis and ***b***-axis is 118.91°.[1, 31] The distorted low-symmetry triclinic structure leads to a feature-rich Raman spectrum (Figure 1B), and the characteristic vibration modes at 124 cm^{-1} (E_g-like mode), 158 cm^{-1} and 176 cm^{-1} (A_g-like modes) can be observed. Figure 1C shows the X-ray diffraction (XRD) pattern of the $ReSe_2$ with

characteristic peaks at 13.8°, 27.9°, 42.4°, 57.7° and 74.2°, corresponding to the $ReSe_2$ (002), (004), (006), (008) and (0010) diffraction. The exfoliated $ReSe_2$ samples present a tendency along two principal axes (***a***- and ***b***- axes) and the typical morphology is presented in Figure 1D.[32] The corresponding selected area electron diffraction (SAED) pattern (inset in Figure 1D) further verifies the single-crystalline characteristic. Figure 1E-F present the high-angle annular dark-field scanning TEM (HAADF-STEM) images of the in-plane structures of the exfoliated $ReSe_2$, where the Re_4 chain and the spacings between two vicinal Re_4 units (0.39 and 0.35 nm) can be observed.

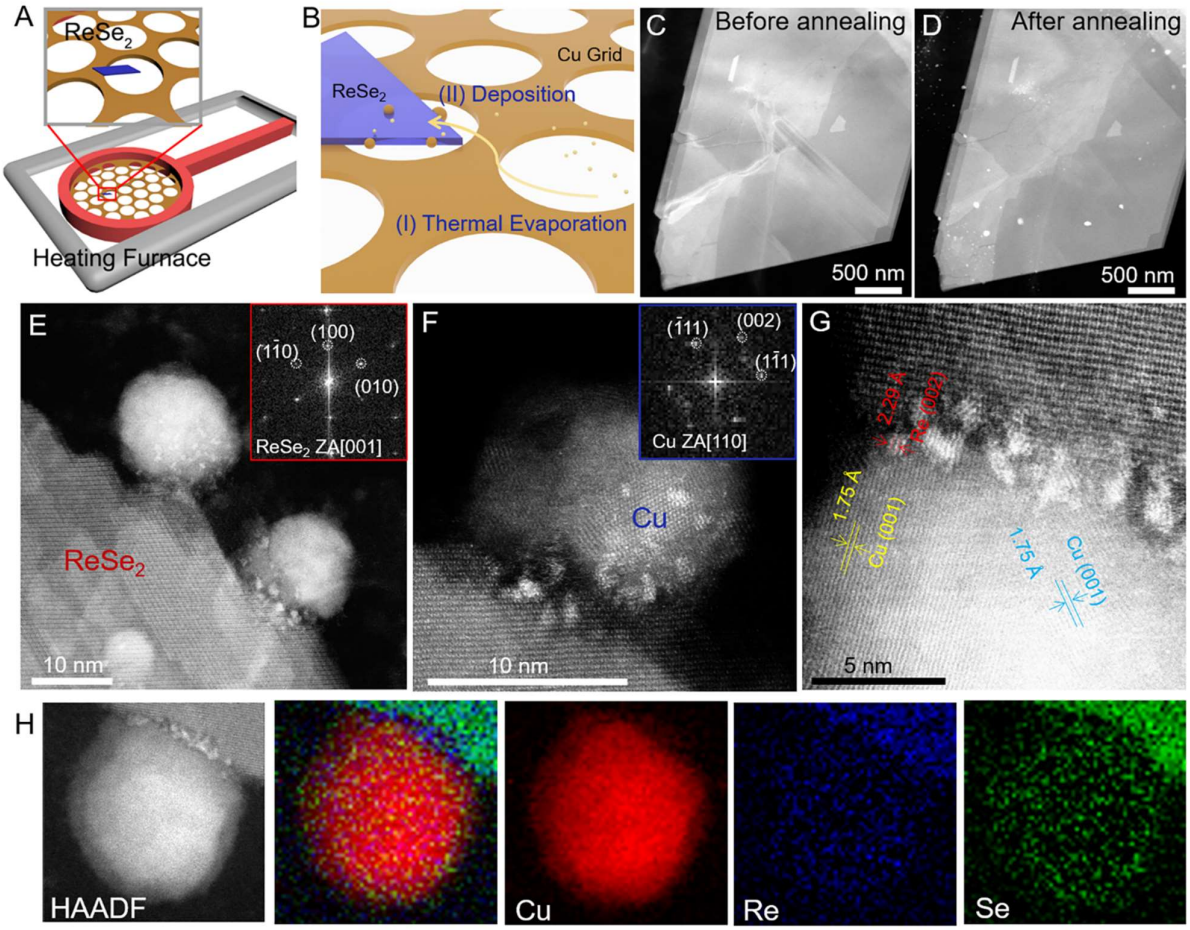

Figure. 2. Cu-$ReSe_2$ contact structure characterization after vacuum annealing. (A) Schematic illustration of the *in-situ* heating experiment. (B) Schematic illustration of the *in-situ* thermal evaporation and deposition of Cu on the $ReSe_2$ flake. The low-mag HAADF-STEM images of the exfoliated $ReSe_2$ (C) before and (D) after vacuum heating at 233-300 °C for 43 min in TEM. (E) HR-STEM image showing the deposited NPs on the edge of $ReSe_2$ flake. Inset is the FFT pattern of the $ReSe_2$ flake. (F) HR-STEM images showing the structure of the deposited Cu NP. Inset is the

corresponding FFT pattern. (G) HR-STEM image of the Cu-$ReSe_2$ interface structure. (H) STEM-EELS mapping of Cu, Re and Se distribution of the reacted interfacial structure.

To investigate the influence of annealing on the contact structure, the exfoliated $ReSe_2$ flakes were transferred to a Cu microgrid and loaded onto the *in-situ* heating holder, which served as a heating furnace surrounding the sample (Figure 2A). Here, the Cu-$ReSe_2$ contact is *in-situ* formed in the TEM through the thermal evaporation and deposition method. As demonstrated in Figure 2B, during the heating process, the Cu species can evaporate from the Cu grid and deposit onto the $ReSe_2$ flakes. As compared in Figure 2C-D, after heating at 233~300 ^oC for 43 min in TEM, many nanoparticles (NPs) with sizes of 5~15 nm attached on the surface and edges of the $ReSe_2$ flake (Figure 2E). Our HAADF-STEM characterizations (Figure 2F) further identified these NPs as Cu. Additionally, many small NPs with ~1 nm size appeared at the Cu/$ReSe_2$ (010) and Cu/$ReSe_2$ (100) interfaces (Figure 2E-G, Figure S1). The small NPs were identified as Re and its (002) plane tend to align with the Cu (001) plane (Figure 2G, Figures S1) possibility due to their smaller lattice mismatch (Figure S2, Tables S1 and Table S2). The STEM-EELS mappings further confirmed the thin Re layer at the interface region (Figure 2H). Additionally, the Se distribution in Cu NP also suggests the accompanied diffusion of Se from $ReSe_2$ to Cu. Thermal decomposition of TMDs typically leads to the evaporative removal of chalcogen atoms and the formation of nanoporous metals. $ReSe_2$ exhibits good thermal stability and the minimum temperature required to initiate Re formation through chalcogen removal is ~950^oC in the H_2/Ar atmosphere.[33, 34] Therefore, we infer that Cu can lower the decomposition temperature of $ReSe_2$ and promote the diffusion of Se atoms.

We then conducted *in-situ* TEM heating experiment to directly reveal the microscopic reaction mechanism at the Cu-$ReSe_2$ contact. With the *in-situ* thermal evaporation and deposition method, we constructed a Cu-$ReSe_2$ contact on the $ReSe_2$ (100) edge (Figure 3A-C). Figure 3D shows a time series of HR-STEM images depicting the structure evolution of the Cu-$ReSe_2$ interface at 450 ^oC. It is noted that the Cu NP was pinned at its original site and didn't migrate during this process. The yellow dashed lines in Figure 3D indicate the interface location between Re NPs and the intact $ReSe_2$. Based on our observations, we plotted the number of consumed Re_4 chains as a function of annealing time increase (Δt) in Figure 3E, and six Re_4 chains were consumed in 50 mins. In the meanwhile, the generated Re NPs grown and coalesced to a continuous thin film (thickness increased from 1.17 nm to 3.82 nm) (Figure 3D).

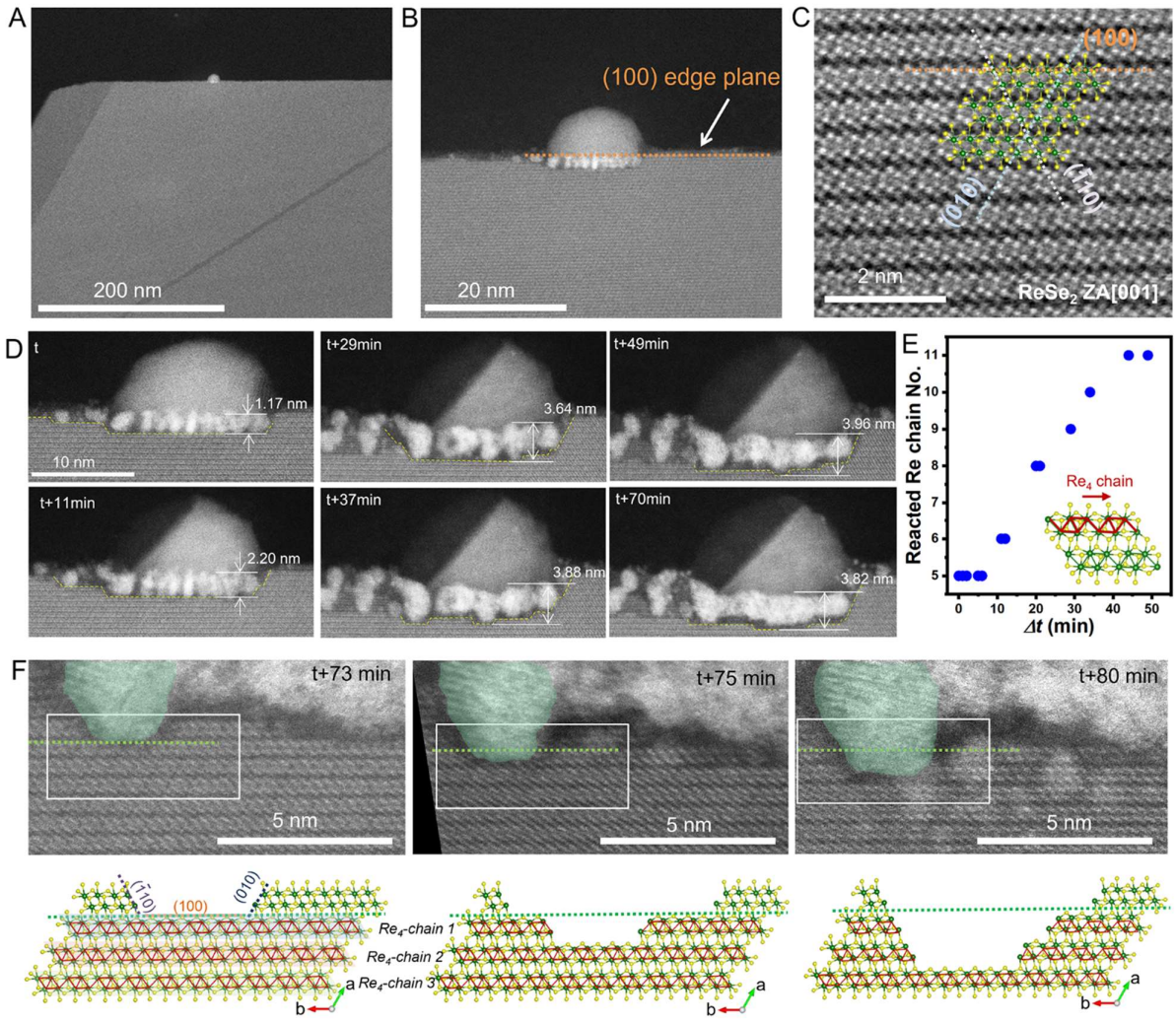

Figure. 3. In-plane reaction behavior of $ReSe_2$ with Cu during the vacuum annealing at 450 ºC. (A) Low and (B) High-mag STEM images of the *in-situ* deposited Cu NP on the edge plane of the $ReSe_2$ flake. (C) HR-STEM image of the $ReSe_2$ flake obtained from [001] zone axis. The crystal structure of $ReSe_2$ is also superimposed. (D) The time series of HR-STEM images of the interfacial structure of the Cu-$ReSe_2$ contact. The yellow dashed lines indicate the Re-$ReSe_2$ interface. (E) The relationship between the consumed Re chain number and annealing time increase (Δt). (F) HR-STEM images and atomic models of the interfacial structure at the Cu-$ReSe_2$ contact from the white framed region.

As presented in the framed region in Figure 3F, in $ReSe_2$ (001) basal plane, two Re_4 chains were consumed in 7 mins (from *t*+73 mins to *t*+80 mins) with a chain-by-chain manner. This is mainly caused by the lowest energy of edges along the ***b*** axis, where only 4 Re-Se bonds need to be broken

per unit cell length.[35] Meanwhile, the $ReSe_2$ (100), $(\bar{1}10)$ and (010) facets were always exposed. According to our calculations (Table S3), $ReSe_2$ (100) and $(\bar{1}10)$ planes possess relatively lower surface energies (0.75 and 1.29 J/m^2). With a relatively higher surface energy (1.63 J/m^2), the $ReSe_2$ (010) plane possesses a higher Re-Se bond density and more Se can be provided for the reactions (Table S3, Figure S3).

It should be mentioned that the Re NPs were also observed at regions surrounding the deposited Cu NP (Figure S4). As compared in the framed region in Figure 4A and B, a new NP (indicated by the white arrow in Figure 4B) formed and these NPs were identified as Re (Figure S5, Figure 2G-H). According to the Z-contrast image intensity profile along the dashed framed region in Figure 4C (Figure 4D), the reacted regions of $ReSe_2$ presented a lower image intensity than the intact region, suggesting a relatively lower scattering (or thinner sample thickness). Considering the relatively week van der Waals interaction between $ReSe_2$ (001) layers, the observed thinner thickness of the reacted $ReSe_2$ indicates that the Re NP was formed by consuming the top $ReSe_2$ (001) layer and the reaction also occurred through a "layer-by-layer" mode. HRTEM and STEM-EELS characterization of the annealed Cu-$ReSe_2$ contact (Figure S6 and Figure 4E) further confirmed the formation of Re and the diffusion of Se from the surrounding $ReSe_2$ into Cu. The Cu NP act as a "sink" for the Se species, leading to the decomposition of $ReSe_2$ surrounding the deposited Cu NP.

To reveal the underlying mechanisms of the Cu-$ReSe_2$ interfacial reactions, we further conducted theoretical calculations by using the Cu atom adsorbed on $ReSe_2$ (100) edge plane as a model and the most stable configurations are presented in Figure S7 and Figure S8. This idealized model provides a direct description of the interaction between a single Cu atom and $ReSe_2$, thereby offering insights into the influence of Cu on the chemical bonds in $ReSe_2$. The existence of the attached Cu atom can change the coordination environment and results in charge redistribution. As presented in Figure 4F and Table S4, our Bader charge analysis reveals a charge transfer of 0.32*e* from Cu to the adjacent Se atoms (Figure 4F). Moreover, these transfers also found between Re and Se atoms (Table S4), indicating the electron redistribution and chemical bond rebuild. Additionally, our projected crystal orbit Hamilton population (pCOHP) analysis further showed that the introduction of a Cu atom inhibited the anti-bonding interaction for Re-Se around Fermi level (Figure 4G), suggesting the stability of the Cu absorbed system, which is consistent with Cu adsorption energy of -1.92 eV. The

energy integrated COHP (ICOHP) values was also calculated (Table S5), which can be used to estimate the bond energy, *i.e.* the more negative value and the stronger bonding strength.[36] Clearly, Cu adsorption decrease the ICOHP value of Re-Se (Figure 4G), indicates the lowered bonding strength of Re-Se.

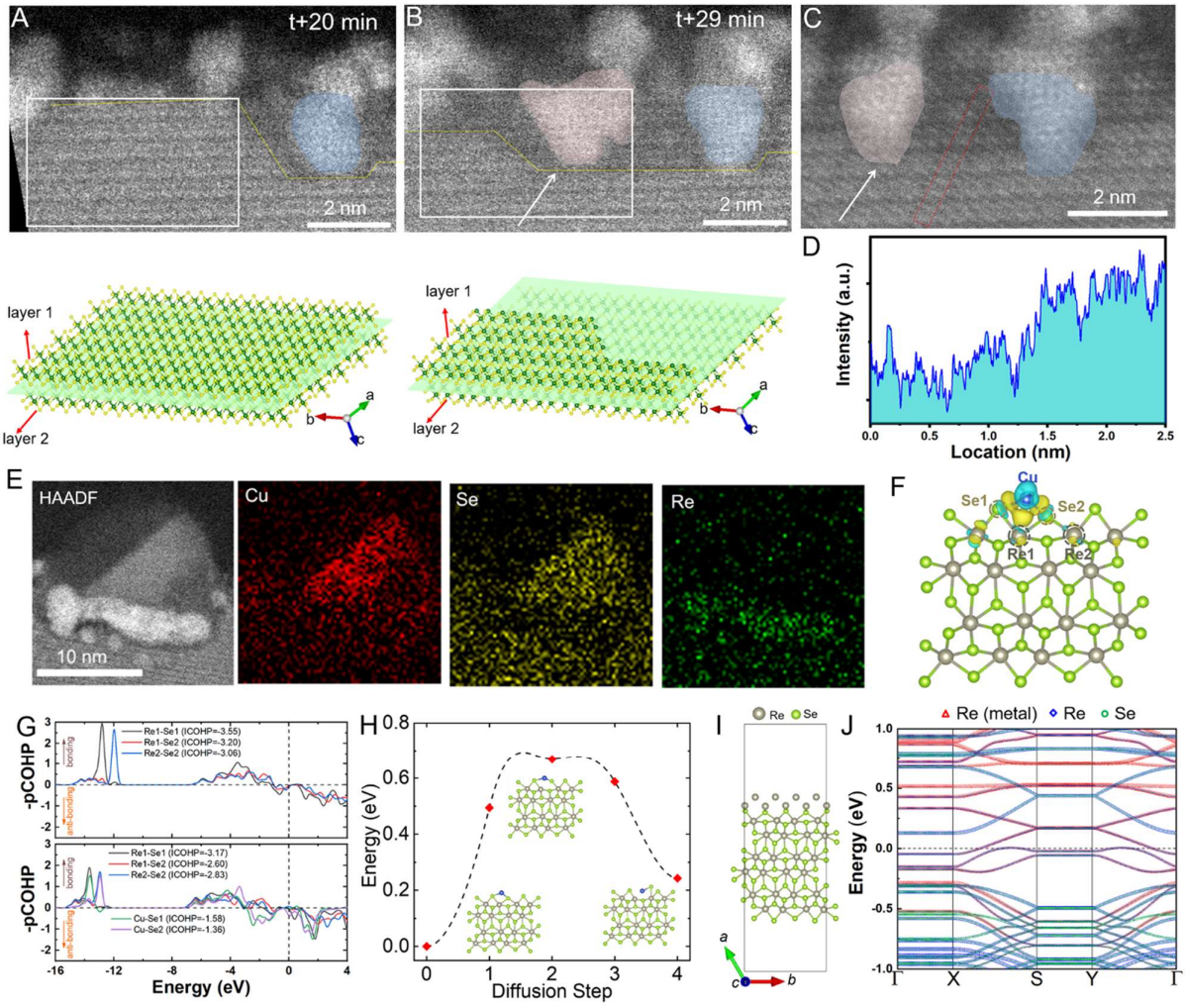

Figure. 4. Formation of Re NPs from $ReSe_2$ through the diffusion of Se toward Cu. HR-STEM images of the reacted $ReSe_2$ after *in-situ* annealing for (A) t+20 min, (B) t+29 min and (C) t+26 min, the white arrows in B and C denote the same formed Re NP evolved from A. The corresponding atomic models are also presented in A and B. (D) Z-contrast image intensity profile along the dashed framed region in C, showing the distinct contrast variation among the reacted and non-reacted regions. (E) STEM-EELS mapping of the annealed Cu-$ReSe_2$ contact in Figure 3. (F) Calculated charge difference of Cu-$ReSe_2$. The isosurface with yellow and cyan color refer to the gain and decrease of electrons, respectively. (G) Projected Crystal Orbit Hamiton Population (pCOHP) and integrated COHP for

$ReSe_2$ and Cu-$ReSe_2$. (H) Minimum energy pathway for the diffusion of Se atom from $ReSe_2$ layer to the Cu NPs. The inert are initial, intermediate and final states of Se atom. (I) Crystal structure and (J) corresponding electronic band structure for Re/$ReSe_2$ heterostructure.

The climbing image nudged elastic band (CI-NEB) method was adopted to evaluate the diffusion energy barrier of Se atom. As presented in Figure 4H. The energy barrier for Se atom to diffuse from $ReSe_2$ into Cu is ~0.69 eV, which is significantly lower than that without Cu atom (~1.83 eV, Figure S9). This value is also lower than the diffusion energy of chalcogen atoms or vacancies in other TMDs (Figure S10).[37-39] It should be mentioned that the generally accepted threshold for CO oxidation at room temperature is 0.80 eV.[40-42] Moreover, according to Tandon *et al.*, the diffusion energy for substituted boron in diamond (1.5 eV) corresponds to a diffusion initiation temperature of 310°C.[43] These results suggest that the energy barrier of ~0.69eV can be crossed during our annealing process. Therefore, the introduction of Cu atoms can prompt the Re-Se bond breaking and facilitate the Se atom diffusion toward Cu.

We future evaluated the influence of the Re interlayer on the electrical transport properties of $ReSe_2$ device by constructing Re/$ReSe_2$ heterostructure (Figure 4I and Figure S11A). As compared in Figure 4J and Figure S11B, the calculated electronic band structures respectively suggest the semiconductor and metal-like character of $ReSe_2$ and Re/$ReSe_2$ heterostructure, indicating a better electrical transport property of the Re/$ReSe_2$ heterostructure. Atomic scale electronic band structure indicates the Fermi level crossed bands are mainly contributed from Re layer (Figure 4J). To verify the influence of the vacuum annealing on the device performance, we fabricated $ReSe_2$ devices with two Cu electrodes. According to the current-voltage (*I-V*) characteristics (Figure S12A), a linear I-V curve was obtained after the vacuum annealing process, indicating that the Schottky contact of the as-fabricated device has been transformed to Ohmic contact. The work function of polycrystalline Cu and Re are 4.65 eV and 4.96 eV, respectively.[44] The Fermi energy of $ReSe_2$ layers is reported to be 4.77 eV,[45] and the conduction band minimum and valence band maximum of $ReSe_2$ have been reported to at 3.90 eV and 5.02 eV (Figure S12B).[46] Figure S12C and D present the energy band alignment of the $ReSe_2$ with Cu and Re electrode. Due to the relatively smaller work function of Cu than Re, $ReSe_2$ will respectively form Schottky and Ohmic contact with Cu and Re. As a rare metal, Re can offer good electrical conductivity, excellent wear resistance and arc erosion resistance. The

Re-based ohmic contacts, with their lower annealing temperature, has been reported to offer a promising alternative to Ti-Al contacts.[47, 48] Moreover, Re provide a good contact resistance stability at extremely high temperature (up to 1300 ºC) and oxidizing conditions.[49-51] Here, we developed a novel method to form the Re ohmic contact with $ReSe_2$ by utilizing the interfacial reaction between Cu and $ReSe_2$ at low-temperature vacuum annealing.

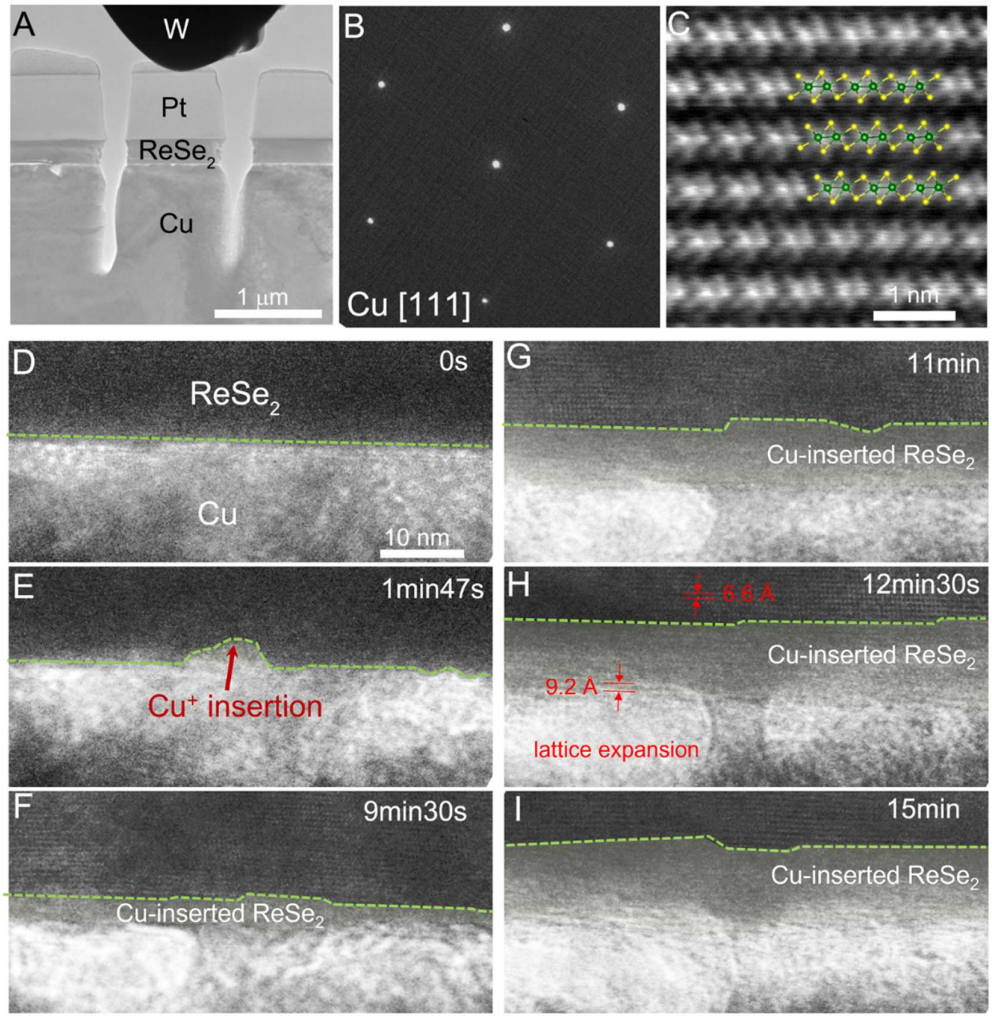

Figure.5. Cu-$ReSe_2$ interfacial reactions under electrical measurement**.** (A) Experimental setup for the *in-situ* biasing experiment. (B) SAED pattern of the Cu substrate captured from the [111] zone axis. (C) HR-STEM image of the layered $ReSe_2$ viewed along the [010] direction. The HRTEM images of the $ReSe_2$-Cu interfacial structure (D) before (dotted line indicate the interface) and (G-I) during the electrical measurement. The dotted lines indicate the interface between Cu-inserted $ReSe_2$ and pristine $ReSe_2$.

To reveal the Joule heating effect on the structural stability of Cu-$ReSe_2$ contact, we further

conducted *in-situ* biasing experiment on a Cu/$ReSe_2$/Pt device (Figure 5A and Figure S13), which was constructed by transferring the exfoliated $ReSe_2$ flakes onto a single crystalline Cu substrate (Figure 5B) and lifted out with standard FIB process. Prior to the electrical measurement, the $ReSe_2$ possessed pristine layered structure (Figure 5C) and a flat interface with Cu (denoted by the dotted green line in Figure 5D). Under the electric measurement, Cu atoms can be oxidized to Cu^+ and embedded in the $ReSe_2$ interlayers, due to the large interlayer spacing of $ReSe_2$ (6.6 Å). As presented in Figure 5E-I, we found that the intercalation depth of Cu^+ into $ReSe_2$ is gradually increased with time, while no Re NPs or interlayers formed at the contact region. The induced local lattice distortion and expansion (6.6 Å vs. 9.2 Å, Figure 5H) resulted in clear interfaces with the intact $ReSe_2$ (dotted lines in Figure 5E-I). When we further increased the I_{CC}, Cu^+ gradually migrated on the $ReSe_2$ surface (Figure S14) and formed a Cu filament, leading to a significant current increase (Figure S14B). In the thermal annealing process, the attached Cu atoms can facilitate the chemical bond breaking of $ReSe_2$ and lower the Se diffusion energy barrier toward Cu, resulting in the formation of interfacial Re layers in between Cu and $ReSe_2$. However, unlike the pinning behavior of Cu in the *in-situ* heating experiment (Cu pinned at its original site and didn't migrate on $ReSe_2$, Figure 3), Cu preferred to migrate on the edge side of $ReSe_2$ under electric field (Figure S14). Hence, we conclude that the electrical measurement can only lead to the migration and intercalation of Cu^+.

Conclusion

In summary, we have dynamically revealed the interfacial reaction between Cu and $ReSe_2$ during the high vacuum annealing process through *in-situ* heating experiments in TEM. The $ReSe_2$ underneath and near the Cu exhibits "chain-by-chain" and "layer-by-layer" etching behaviors at temperatures ~300ºC. The etching mechanism is identified as the diffusion of Se atoms into Cu, resulting in the formation of a thin, continuous Re interlayer at the contact interface. Theoretical calculations confirm that Cu atoms facilitate the chemical bond breaking in $ReSe_2$, promoting Se diffusion into Cu. The resulting Re-$ReSe_2$ interface presents a metal-like electronic band structure, which contributes to improved contact resistance. Our findings provide a potential strategy to form ohmic contact for $ReSe_2$-based devices, especially for their reliable applications at high-temperatures and in oxidizing conditions.

ASSOCIATED CONTENT

Supporting Information

The Supporting Information is available free of charge at …

Experimental methods, additional characterizations of the annealed interfacial structures, theoretical calculation models and results, and in-situ biasing results (PDF).

AUTHOR INFORMATION

Author Contributions

X.L., S.C. and Y.Z. conceived and designed the study. C.S. and Y.Z. supervised the project. X.L., W.Y. and S.C. performed the *in-situ* heating/biasing experiments and TEM characterizations. X.L. and S.C. analyzed the data. D.W. conducted the theoretical calculations. W.H., W.Y. and Y.G. fabricated the devices and measured its electrical properties. All the authors participate in discussions and provide comments on the manuscript. X.L., W.Y. and D.W. contributed equally to this work.

Notes

The authors declare no competing financial interests.

ACKNOWLEDGMENTS

This work was supported by the National Natural Science Foundation of China (Nos. 52072345, 12274371, 62271450, 12204156), Young Elite Scientists Sponsorship Program by CAST (No. 2023QNRC001), and the China Postdoctoral Science Foundation (Nos. 2023QT0315, 2023M743223). Electron microscopy work at BNL was supported by DOE-BES, Materials Science and Engineering Division and Center for Functional Nanomaterials, under Contract No. DE-SC0012704. This work is also supported by the National Supercomputing Center in Zhengzhou, Henan.

REFERENCES

[1] Zhang, E.; Wang, P.; Li, Z.; Wang, H.; Song, C.; Huang, C.; Chen, Z.-G.; Yang, L.; Zhang, K.; Lu, S.; et al. Tunable ambipolar polarization-sensitive photodetectors based on high-anisotropy $ReSe_2$ nanosheets. *ACS Nano* **2016**, 10, 8067-8077.

[2] Yang, S.; Wang, C.; Sahin, H.; Chen, H.; Li, Y.; Li, S.-S.; Suslu, A.; Peeters, F. M.; Liu, Q.; Li, J.; et al. Tuning the optical, magnetic, and electrical properties of $ReSe_2$ by nanoscale strain engineering. *Nano Lett.* **2015**, 15, 1660-1666.

[3] Ran, J.; Chen, L.; Wang, D.; Talebian‐Kiakalaieh, A.; Jiao, Y.; Hamza, M. A.; Qu, Y.; Jing, L.; Davey, K.; Qiao, S.-Z. Atomic-level regulated 2D $ReSe_2$: a universal platform boostin photocatalysis. *Adv. Mater.* **2023**, 35, 2210164.

[4] Kim, J.; Heo, K.; Kang, D.-H.; Shin, C.; Lee, S.; Yu, H.-Y.; Park, J.-H. Rhenium diselenide ($ReSe_2$) near-infrared photodetector: performance enhancement by selective p-Doping technique. *Adv. Sci.* **2019**, 6, 1901255.

[5] Park, J. Y.; Joe, H.-E.; Yoon, H. S.; Yoo, S.; Kim, T.; Kang, K.; Min, B.-K.; Jun, S.C. Contact effect of ReS_2/metal interface. *ACS Appl. Mater. Interfaces* **2017**, 9, 26325-26332.

[6] Rahman, M.; Davey, K.; Qiao, S.-Z. Advent of 2D rhenium disulfide (ReS_2): fundamentals to applications. *Adv. Funct. Mater.* **2017**, 27, 1606129.

[7] Abraham, M.; Mohney, S. E. Annealed Ag contacts to MoS_2 field-effect transistors. *J. Appl. Phys.* **2017**, 122, 115306.

[8] Khan, M. F.; Rehman, S.; Akhtar, I.; Aftab, S.; Ajmal, H. M. S.; Khan, W.; Kim, D.-k.; Eom, J. High mobility $ReSe_2$ field effect transistors: Schottky-barrier-height-dependent photoresponsivity and broadband light detection with Co decoration. *2D Mater.* **2019**, 7, 015010.

[9] Aftab, S.; Samiya, M.; Hussain, M. S.; Elahi, E.; Yousuf, S.; Ajmal, H. M. S.; Iqbal, M.W.; Iqbal, M.Z. $ReSe_2$/metal interface for hydrogen gas sensing. *J. Colloid Interface Sci.* **2021**, 603, 511-517.

[10] Feng, Q.; Li, L.-M.; Hao, Y.; Ni, J.-Y.; Zhang, J.-C. The improvement of ohmic contact of Ti/Al/Ni/Au to AlGaN/GaN HEMT by multi-step annealing method. *Solid State Electron* **2009**, 53, 955-958.

[11] Chen, X.; Xu, J.; Mao, S.; He, Y.; Gao, J.; Liu, W.; Sun, X.; Wang, G.; Zhao, C.; Luo, J. Enhanced thermal stability and reduced specific contact resistivity in titanium-based ohmic contact with an ultra-thin molybdenum interlayer. *IEEE Electron Device Lett* **2024**, 45, 1281-1284.

[12] Kim, M.-S.; Hwang, S.-H.; Kim, S.-H.; Kim, J.-H.; Park, E.; Han, K.-H.; Yu, H.-Y. Excellent improvement of contact resistivity and thermal stability for high temperature process after silicidation of $TiSi_2$ through Ta interlayer for diffusion barrier. *IEEE Electron Device Lett* **2023**, 44, 1040-1043.

[13] Lee, M.-H.; Peterson, R. L. Interfacial reactions of titanium/gold ohmic contacts with Sn-doped β-Ga_2O_3. *APL Mater.* **2019**, 7, 022524.

[14] Kappera, R.; Voiry, D.; Yalcin, S. E.; Branch, B.; Gupta, G.; Mohite, A. D.; Chhowalla, M. Phase-

engineered low-resistance contacts for ultrathin MoS_2 transistors. *Nat. Mater.* **2014**, 13, 1128-1134.

[15] Feng, W.; Zhou, X.; Tian, W. Q.; Zheng, W.; Hu, P. A. Performance improvement of multilayer InSe transistors with optimized metal contacts. *Phys. Chem. Chem. Phys.* **2015**, 17, 3653-3658.

[16] Leong, W. S.; Nai, C. T.; Thong, J. T. L. What does annealing do to metal-graphene contacts?. *Nano Lett.* **2014**, 14, 3840-3847.

[17] Zhou, L.; Sun, Y. H.; Wu, Y. S.; Zhu, Y.; Xu, Y.; Jia, J.; Wang, F.; Wang, R. Controlled growth of Pd nanocrystals by interface interaction on monolayer MoS_2: An atom-resolved in situ study. *Nano Lett.* **2023**, 23, 11360−11367.

[18] Park, H.; Son, J.; Kim, J. Reducing the contact and channel resistances of black phosphorus via low-temperature vacuum annealing. *J. Mater. Chem. C* **2018**, 6, 1567-1572.

[19] English, C. D.; Shine, G.; Dorgan, V. E.; Saraswat, K. C.; Pop, E. Improved contacts to MoS_2 transistors by ultra-high vacuum metal deposition. *Nano Lett.* **2016**, 16, 3824-3830.

[20] Dai, J.; Sun, Y.; Liu, Z.; Zhang, Y.; Duan, S.; Wang, R. Using in situ transmission electron microscopy to study strong metal-support interactions in heterogeneous catalysis. *Angew. Chem. Int. Ed.* **2024**, 63, e202409673.

[21] Kang, J.; Liu, W.; Banerjee, K. High-performance MoS_2 transistors with low-resistance molybdenum contacts. *Appl. Phys. Lett.* **2014**, 104, 093106.

[22] Schulman, D. S.; Arnold, A. J.; Das, S. Contact engineering for 2D materials and devices. *Chem. Soc. Rev.* **2018**, 47, 3037-3058.

[23] Corbet, C. M.; Sonde, S. S.; Tutuc, E.; Banerjee, S. K. Improved contact resistance in $ReSe_2$ thin film field-effect transistors. *Appl. Phys. Lett.* **2016**, 108, 162104.

[24] Souder, A.; Brodie, D. E. Electrical contacts and conductivity of MoS_2 layer structures. *Can J Phys* **1971**, 49, 2565-2571.

[25] Zhu, Y.; Sun, Y.; Zhao, Z.; Xu, Y.; Li, H.; Wang, R. Atomic scale in-situ observation of gas-solid interaction regulating the pre-nucleation process of Pd atomic clusters. *Nano Today* **2024**, 59, 102533.

[26] Zhao, H.; Zhu, Y.; Ye, H.; He, Y.; Li, H.; Sun, Y.; Yang, F.; Wang, R. Atomic-scale structure dynamics of nanocrystals revealed by in situ and environmental transmission electron microscopy. *Adv. Mater.* **2023**, 35, 2206911.

[27] Wang, R. The dynamics of the peel. *Nat. Catal.* **2020**, 3, 333–334.

[28] Rehman, S.; Kim, H.; Khan, M. F.; Hur, J.-H.; Eom, J.; Kim, D.-k. Tunable resistive switching of vertical $ReSe_2$/graphene hetero-structure enabled by Schottky barrier height and DUV light. *J. Alloys Compd.* **2021**, 855, 157310.

[29] Liu, X.-C.; Zhao, S.; Sun, X.; Deng, L.; Zou, X.; Hu, Y.; Wang, Y.-X.; Chu, C.-W.; Li, J.; Wu, J.; et al. Spontaneous self-intercalation of copper atoms into transition metal dichalcogenides. *Sci. Adv.* **2020**, 6, eaay4092.

[30] Stern, C.; Twitto, A.; Snitkoff, R. Z.; Fleger, Y.; Saha, S.; Boddapati, L.; Jain, A.; Wang, M.; Koski, K. J.; Deepak, F. L.; et al. Enhancing light–matter interactions in MoS_2 by copper intercalation. *Adv. Mater.* **2021**, 33, 2008779.

[31] Lamfers, H. J.; Meetsma, A.; Wiegers, G. A.; de Boer, J. L. The crystal structure of some rhenium and technetium dichalcogenides. *J. Alloys Compd.* **1996**, 241, 34-39.

[32] Wang, H.; Liu, E.; Wang, Y.; Wan, B.; Ho, C.-H.; Miao, F.; Wan, X. G. Cleavage tendency of anisotropic two-dimensional materials: ReX_2 (X = S,Se) and WTe_2. *Phys. Rev. B* **2017**,96, 165418.

[33] Jariwala, B.; Thamizhavel, A.; Bhattacharya, A. ReSe2: a reassessment of crystal structure and thermal analysis. *J. Phys. D.* **2017**, 50, 044001.

[34] Chatterjee, S.; Anikin, A.; Ghoshal, D.; Hart, J. L.; Li, Y.; Intikhab, S.; Chareev, D.A.; Volkova, O.S.; Vasiliev, A.N.; Taheri, M. L.; Koratkar, N.; Karapetrov, G.; Snyder. J. Nanoporous metals from thermal decomposition of transition metal dichalcogenides. *Acta Materialia* **2020**, 184, 79-85.

[35] Chen, X.; Lei, B.; Zhu, Y.; Zhou, J.; Liu, Z.; Ji, W.; Zhou, W. Pristine edge structures of T″-phase transition metal dichalcogenides ($ReSe_2$, ReS_2) atomic layers. *Nanoscale* **2020**, 12, 17005-17012.

[36] Tang, G.; Yang, C.; Stroppa, A.; Fang, D.; Hong, J. Revealing the role of thiocyanate anion in layered hybrid halide perovskite $(CH_3NH_3)_2Pb(SCN)_2I_2$. J. Hong, *J. Chem. Phys.* **2017**, 146, 224702.

[37] Li, S.; Lin, J.; Chen, Y.; Luo, Z.; Cheng, H.; Liu, F.; Zhang, J.; Wang, S. Growth Anisotropy and Morphology Evolution of Line Defects in Monolayer MoS_2: Atomic-Level Observation, Large-Scale Statistics, and Mechanism Understanding. *Small* **2024**, 20, 2303511

[38] Ullah, H.; Noor-A-Alam, M.; Kim, H. J.; Shin, Y. H. Influences of vacancy and doping on electronic and magnetic properties of monolayer SnS. *J. Appl. Phys.* **2018**, 124, 065102

[39] Zhang, S.; Li, M. L.; Jiang, M.; Xiao, H. Y.; Scanlon, D. O.; Zu, X. T. Formation and migration of vacancy defects in GeSe and SnSe. *J. Phys. B: At. Mol. Opt. Phys.* **2021**, 54 035003

[40] Young, D. Computational Chemistry: A Practical Guide for Applying Techniques to Real World Problems. *Wiley* **2004**.

[41] Deng, Q.; Zhao, L.; Gao, X.; Zhang, M.; Luo, Y.; Zhao, Y. Single layer of polymeric cobalt phthalocyanine: Promising low-cost and high-activity nanocatalysts for CO oxidation. *Small* **2013**, 9, 3306-3513.

[42] Yang, X.; Lu, Z.; Cheng, C.; Wang, Y.; Zhang, X.; Yang, Z.; Lu, W. Identification of efficient single-atom catalysts based on V_2CO_2 MXene by ab Initio Simulations. *J. Phys. Chem. C* **2020**, 124, 4090-4100.

[43] Tandon, N; Grotjohn, T. A; Albrecht, J. D. Evaluating diffusion barriers of defects in boron ion implanted diamond. *Diamond Relat. Mater.* **2024**, 141, 110691.

[44] Michaelson, H. B. The work function of the elements and its periodicity. *J. Appl. Phys.* **1977**, 48, 4729-4733.

[45] Jo, S.-H.; Lee, H. W.; Shim, J.; Heo, K.; Kim, M.; Song, Y. J.; Park, J.-H. Highly efficient infrared photodetection in a gate-controllable van der waals heterojunction with staggered bandgap alignment. *Adv. Sci.* **2018**, 5, 1700423.

[46] Ozcelik, V. O.; Azadani, J. G.; Yang, C.; Koester, S. J.; Low, T. Band alignment of two-dimensional semiconductors for designing heterostructures with momentum space matching. *Phys. Rev. B* **2016**, 94, 035125.

[47] Shah, A. P.; Chalke, B. A.; Mhatre, V. J.; Bhattacharya, A. Rhenium-based low resistivity and low annealing temperature ohmic contacts to n-GaN. *J. Appl. Phys*. **2022**, 132, 075701.

[48] McDaniel, G. Y.; Fenstermaker, S. T.; Lampert, W. V.; Holloway, P. H. Rhenium ohmic contacts on 6H-SiC. *J. Appl. Phys.* **2004**, 96, 5357-5364.

[49] Carlen, J. C.; Bryskin, B. D. Rhenium-A Unique Rare Metal. *Mater. Manuf. Processes* **1994**, 9 1087-1104.

[50] Liu, Q. Z; Lau, S. S. A review of the metal-GaN contact technology. *Solid-State Electron.* **1998**, 42, 677-691.

[51] Mohney, S. E.; Liu, X. Estimated phase equilibria in the transition metal-Ga-N systems: Consequences for electrical contacts to GaN. *J. Elect. Mat.* **1996**, 25, 811.

TOC Graphic

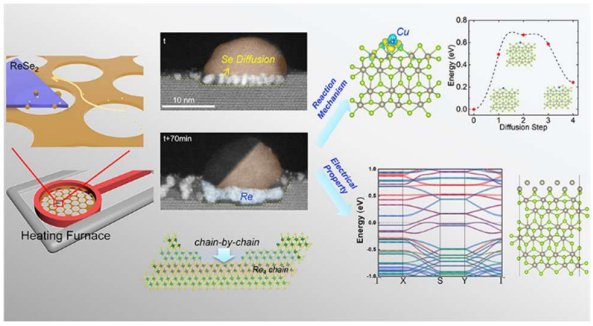
ReSe2
Heating Furnace
t
Se Diffusion
10 nm
t+70min
Re
chain-by-chain
Re4 chain
Cu
Reaction Mechanism
Energy (eV)
Diffusion Step
Electrical Property
Energy (eV)
Γ
X
S
Y
Γ